Phys Chem Minerals (2004) 31: 22–27
DOI 10.1007/s00269-003-0330-6

ORIGINAL PAPER

Y. Lee · J. A. Hriljac · A. Studer · T. Vogt

Anisotropic compression of edingtonite and thomsonite to 6 GPa at room temperature

Received: 16 January 2003 / Accepted: 24 April 2003

Abstract Polycrystalline samples of natural edingtonite (New Brunswick, Canada) and thomsonite (Oregon, USA) were studied up to 6 GPa using monochromatic synchrotron X-ray powder diffraction and a diamond-anvil cell with a methanol:ethanol:water mixture as a penetrating pressure-transmitting fluid. Unlike natrolite, previously studied under the same conditions, edingtonite and thomsonite do not show any apparent pressure-induced hydration (PIH) or phase transitions. All these fibrous zeolites are characterized by their anisotropic compressibilities, with the linear compressibilities of the fibrous chains (*c*-axis) being as small as one third of those perpendicular to the chains (*a*-, *b*-axes); for edingtonite, $\beta_0^a = 0.0050(3)$ GPa^{-1}, $\beta_0^b = 0.0054(2)$ GPa^{-1}, $\beta_0^c = 0.0034(1)$ GPa^{-1}; for thomsonite, $\beta_0^a = 0.0080(2)$ GPa^{-1}, $\beta_0^b = 0.0084(2)$ GPa^{-1}, $\beta_0^c = 0.0032(1)$ GPa^{-1}. The pressure–volume data were fitted to a second-order Birch–Murnaghan equation of state using a fixed pressure derivative of 4. As a result of the 0000-type connectivity of the chains, the bulk modulus of edingtonite is found to be about 40% larger than that of thomsonite; $K_0^{EDI} = 73(3)$ GPa, $K_0^{THO} = 52(1)$ GPa. Distance least-squares refinements were used to model the expected framework, following the observed linear compression behaviors. The chain-bridging T–O–T angle is proposed to be correlated with the different compressibilities across the chains in each framework type.

Keywords Edingtonite · Thomsonite · High pressure · Anisotropic compression · Bulk modulus · Distance least-squares

Y. Lee · T. Vogt (✉)
Physics Dept., Brookhaven National Laboratory,
Upton, New York 11973–5000, USA
E-mail: yollee@bnl.gov, tvogt@bnl.gov
Tel: +1-631-344-8485; Fax: +1-631-344-2739

J. A. Hriljac
School of Chemical Sciences,
The University of Birmingham, Birmingham, B15 2TT, UK

A. Studer
Bragg Institute, ANSTO, PMB 1, Menai, NSW 2234, Australia

Introduction

Zeolites crystallize in a variety of low-density framework structures composed of corner-connected networks of TO_4 (T = Al, Si, Ga...) tetrahedra, which enclose well-defined pores of molecular dimensions containing charge-balancing cations and molecules such as water (Breck 1984). The porous nature built from rigid tetrahedra and flexible T–O–T connectors favors unusual structural behaviors in response to thermodynamic variables such as temperature and pressure. Numerous variable-temperature studies show that cations can migrate within the pores, and water contents vary, usually with a concomitant relaxation of the framework (Parise et al. 1984; Baur and Joswig 1996; Norby et al. 1998; Lee et al. 2001b). Under hydrostatic pressures, some zeolites have been shown to exhibit anomalous compressibility or an increase in water diffusivity when a pore-penetrating pressure medium is used (Hazen, 1983; Belitsky et al. 1992; Moroz et al. 2001). We have recently demonstrated that pressure-induced volume expansion observed in natrolite and its related analogues occurs through the selective sorption of water molecules from the hydrostatic pressure fluid, giving rise to a pressure-induced hydration (PIH) state (Lee et al. 2001a, 2002a,b). Since edingtonite and thomsonite are closely related to natrolite, built from so-called fibrous chains of tetrahedra, their structural responses under pressure will provide an understanding for the comparative crystal chemistry, particularly with respect to PIH, of this class of fibrous zeolites as well as fundamental properties of materials such as bulk modulus and linear compressibility. Although there have been several reports of the high-pressure behavior of zeolites with the natrolite topology (including mesolite and scolecite) (Belitsky et al. 1992; Gillet et al. 1996; Bazhan et al. 1999; Goryainov and Smirnov 2001; Moroz et al. 2001; Lee et al. 2001a, 2002a,b; Ballone et al. 2002; Comodi et al. 2002), to our knowledge there is only a brief mention of a study on edingtonite (Belitsky et al. 1992), which

contains no experimental details, and there are no reports on thomsonite.

Natrolite (NAT), edingtonite (EDI), and thomsonite (THO) all contain similar aluminosilicate chains that run along the crystallographic *c*-axis, and are classified according to the mode of linkage of these chains in the *a, b* planes (Taylor et al. 1933). These chains are composed of 4-1 T_5O_{10} tetrahedra units (Fig. 1). With in each unit, there are four tetrahedra which form a non planar 4-ring perpendicular to the chain axis (*c*). These are 3-connected with respect to linkages within the unit. The remaining tetrahedron is 4-connected within the unit and closes the 4-rings to generate an infinite chain with a repeat distance of 6.6 Å, which is the *c*-cell parameter in an idealized framework. Taylor et al. (1933) proposed that the centers of the 4-connected tetrahedral nodes in the chain can be expressed in eights of the repeat distance along the *c*-axis. Smith (1983) enumerated the combinations of the chains and showed that the three simplest 3-D nets correspond to natrolite, edingtonite and thomsonite. The topological framework of edingtonite exhibits the *0000* arrangement in terms of the heights of the four 4-connected nodes of the cross-linked 4-1 chains, while thomsonite and natrolite frameworks are arranged as *0022* and *2460*, respectively (Fig. 2). Each arrangement of the chains gives rise to the characteristic 3-D channel system within which nonframework cations and water molecules are located. The mineral edingtonite studied here (ideally, $Ba_2Al_4Si_6O_{20}{\cdot}8H_2O$) crystallizes in $P2_12_12$ with $a = 9.525(2)$ Å, $b = 9.640(2)$ Å, $c = 6.504(1)$ Å; thomsonite (ideally, $Na_4Ca_8Al_{20}Si_{20}O_{80}{\cdot}24H_2O$) in *Pncn* with $a = 13.080(4)$ Å, $b = 13.056(2)$ Å, $c = 13.195(2)$ Å.

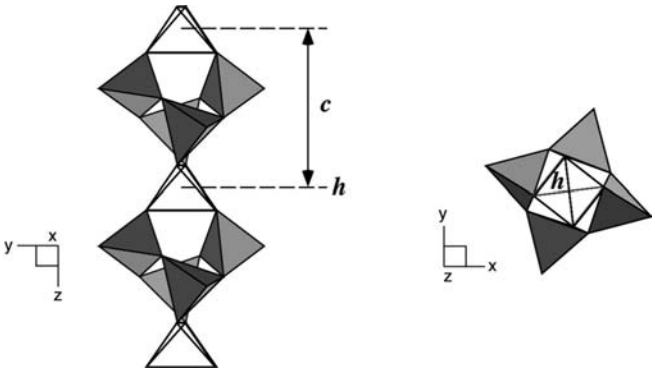

Fig. 1 Polyhedral representations of the chains found in fibrous zeolites. The tetrahedra of the nonplanar 4-rings are shown *shaded*, while the tetrahedra which close the 4-rings are *unshaded*, generating the infinite chain with a repeat distance of 6.6Å (*c*). The relative heights (***h***) from the origin of the centers of the four 4-connected tetrahedral nodes (*unshaded*) in the cross-linked 4-1 chains are arranged differently in natrolite, edingtonite, and thomsonite (see Fig. 2)

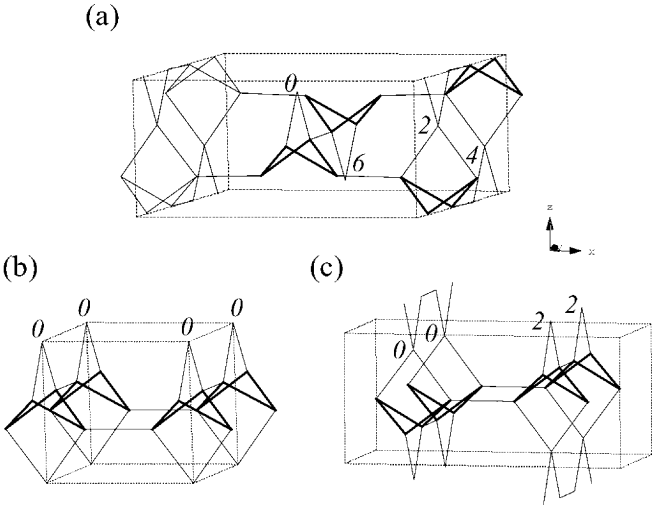

Fig. 2a–c Skeletal representations of the tetrahedral nodes in the topological unit cells of **a** natrolite ($I4_1/amd$, $a = 13.850$ Å, $c = 6.420$ Å); **b** edingtonite ($P\bar{4}m2$, $a = 6.926$ Å, $c = 6.410$ Å); **c** thomsonite ($Pmma$, $a = 14.000$ Å, $b = 7.000$ Å, $c = 6.482$ Å). The heights of the centers of the four 4-connected tetrahedral nodes (see Fig. 1) in each model are shown in terms of eights of the repeat distance. The centers of the tetrahedra of the nonplanar 4-rings are connected with *bold lines*. *Dotted lines* define the unit cells

Experimental

In situ high-pressure synchrotron X-ray powder diffraction:

Experiments were performed using a diamond anvil cell (DAC) at the X7A beamline at the National Synchrotron Light Source (NSLS) at Brookhaven National Laboratory (BNL). The primary white beam from the bending magnet is focused in the horizontal plane by a triangular, asymmetrically cut Si (220) monochromator bent to a cylindrical curvature by applying a load to the crystal tip, affording microfocused (~200 μm) monochromatic radiation of ~0.7 Å (Lemonnier et al. 1978). A tungsten wire cross-hair was positioned at the center of the goniometer circle and subsequently the position of the incident beam was adjusted to the cross-hair. A gas-proportional position-sensitive detector (Smith 1991) was stepped in 0.25° intervals over the angular range of 3–35° with counting times of 90–150 s $step^{-1}$. The wavelength of the incident beam (0.6839(1) Å), PSD zero channel, and PSD degrees $channel^{-1}$ was determined from a CeO_2 standard (SRM 674). Powdered samples of the mineral edingtonite (New Brunswick, Canada NMNH 142990) and thomsonite (Oregon, USA NMNH R12990) were, in turn, loaded into the DAC at ambient pressure and room temperature along with a few small ruby chips. The DAC is based on a modified Merrill–Bassett design (Merrill and Bassett 1974) and employs two diamonds with 0.5-mm diameter culets on tungsten-carbide supports. The X-rays are admitted by a 0.5-mm diameter circular aperture, and the exit beam leaves via a 0.5×3.0-mm rectangular tapered slit, oriented perpendicular to the horizontal plane of the diffractometer. The sample chamber is provided by a 200-μm hole formed in the center of a 250-μm-thick stainless steel gasket, preindented to 100-μm thickness before drilling. A mixture of 16:3:1 by volume of methanol:ethanol:water, which is known to remain hydrostatic up to ~10 GPa, was used as a pressure- transmitting fluid, (Hazen and Finger 1982). The pressure at the sample was measured by detecting the shift in the R1 emission line of the included ruby chips (Bell and Mao 1979). No evidence of nonhydrostatic conditions or pressure anisotropy was detected during our experiments, and the R1 peaks from three to four included ruby chips remained strong and sharp with deviations in the measured pressure of less than ±0.1 GPa. Typically, the sample was equilibrated for about 15 min or more at each measured pressure. The DAC was then placed on the second axis of the diffractometer, and the sample position was adjusted using a precentered microscope. After the diffraction

data measurement, the sample pressure was raised by 0.5 ~ 1.0 GPa increments. Measurements were performed up to 6.3 GPa. The experiments were repeated twice, and in each case the measured diffraction data suffered from sample texture effects and showed some broadening of the peaks at higher pressures. The recovered sample maintained its original white color and crystallinity. Unit-cell parameters were determined by whole pattern fitting using the LeBail method (LeBail et al. 1988: Table 1). The diffraction peaks were modeled by varying only a half-width parameter in the pseudo-Voigt profile function. Bulk moduli were calculated by fitting the Murnaghan equation of state to the normalized volumes

$$V/V_0 = [1 + K'P/K_0]^{-1/K'} \quad ,$$

where $K' = (\partial K/\partial P)_{P=0} = 4$) (Angel, 2000).

Ex situ ambient pressure X-ray powder diffraction:

Data at ambient pressure were measured using dry powder samples of edingtonite and thomsonite in a 0.5-mm glass capillary and monochromatic synchrotron X-ray powder diffraction. In the case of edingtonite, the possibility of volume swelling under different humidity levels was checked using a powder sample, soaked in the same pressure-transmitting fluid as used in the high-pressure experiment, in a 0.5-mm capillary and a Bruker D8 diffractometer, equipped with an incident beam monochromator. Unit-cell volume was determined by whole-pattern fitting using the LeBail method (LeBail et al. 1988; Table 1).

Distance least-squares (DLS):

The use of DLS simulations of crystal structures was discussed by Meier and Villiger (1969) as well as by Baur (1977). In the study of zeolitic structures, these simulations have been used to derive plausible starting models for the refinement of structures with pseudosymmetry (Gramlich and Meier 1971), to test the feasibility of trial models for structure solutions (Olson et al. 1981), and to predict the phase stability of a particular framework topology (Parise et al. 1984). Provided we can determine with confidence more interatomic distances than there are crystallographically independent positional parameters for a particular structure, these distances may be used as observables in a least-squares procedure to predict a crystal structure. The function minimized is:

$$x^2 = \sum_{i=1}^{n} w_i^2 [D_i(\text{predicted}) - D_i(\text{model})]^2 \quad .$$

Here, D_i(model) is the distance between two atoms for a given model, D_i(predicted) is the distance predicted on the basis of the observation of a series of related compounds, and w_i are the weights assigned to the D_i(predicted). Structural studies on framework aluminosilicates have created a database which can be used to optimize the framework geometry at varying cell dimensions. Although the weighting scheme to be used in the procedure is still a matter of debate, it is generally agreed that T–O bond lengths should be given high weights, while O–O and T–T distances should be given lower weights. The framework modeling was performed in $P2_12_12$ and *Pncn* space groups for edingtonite and thomsonite, respectively, using the observed pressure-unit cell data (Table 1).

Results and discussion

The changes of the normalized unit cell lengths and volume of edingtonite and thomsonite are displayed in Fig. 3 as a function of pressure. It is obvious that unlike natrolite, edingtonite and thomsonite do not show apparent volume expansion under the applied hydrostatic conditions mediated by the alcohol and water mixtures; increase in pressure results in volume compression up to 6.3 GPa. In edingtonite, however, the data below 1.5 GPa do not follow the same linear

Table 1 Unit-cell edge lengths and volume of edingtonite and thomsonite at 300 K

Pressure (GPa)[a]	a (Å)	b (Å)	c (Å)	V (Å^3)	DLS-R value[b]	Bridging T–O–T (°)[c]	Chain rotation angle, ψ (°)[c]
Edingtonite ($P2_12_12$)							
0	9.525(2)	9.640(2)	6.504(1)	597.2(3)	0.00256	144.4	25.39
0.67	9.522(2)	9.627(1)	6.502(1)	596.0(1)	0.00258	144.2	25.28
0.98	9.496(3)	9.599(4)	6.492(3)	591.7(3)	0.00272	143.7	24.93
1.29	9.487(4)	9.587(4)	6.484(3)	589.7(3)	0.00283	143.6	24.81
2.17	9.433(3)	9.537(3)	6.459(2)	581.1(2)	0.00317	142.7	24.18
3.32	9.375(3)	9.478(3)	6.435(2)	571.8(2)	0.00352	141.5	23.46
4.00	9.345(3)	9.448(3)	6.416(2)	566.5(3)	0.00379	141.1	23.14
4.78	9.337(4)	9.441(5)	6.415(3)	565.5(4)	0.00381	140.9	23.04
6.24	9.257(11)	9.366(8)	6.378(6)	553.0(7)	0.00436	139.5	22.16
4.20 (on release)	9.336(9)	9.442(9)	6.428(6)	566.6(7)			
2.15 (on release)	9.462(3)	9.563(3)	6.474(2)	585.8(3)			
0 (released)	9.535(2)	9.648(2)	6.511(1)	599.0(1)			
0 (wet)	9.5350(3)	9.6487(3)	6.5100(3)	598.9(1)			
Thomsonite (*Pncn*)							
0	13.080(4)	13.056(2)	13.195(2)	2253.4(11)	0.00291	135.0	20.03
0.31	13.069(1)	13.033(2)	13.194(1)	2247.3(3)	0.00295	134.7	19.90
1.09	12.985(2)	12.959(2)	13.159(1)	2214.2(3)	0.00324	133.8	19.27
1.50	12.945(1)	12.910(2)	13.139(1)	2195.8(4)	0.00340	133.3	18.93
2.17	12.888(2)	12.850(2)	13.110(1)	2171.2(4)	0.00363	132.7	18.50
3.04	12.814(3)	12.789(5)	13.075(2)	2142.5(7)	0.00391	132.0	18.01
4.36	12.708(6)	12.683(9)	13.018(3)	2098.3(13)	0.00435	130.9	17.26
5.25	12.627(4)	12.556(15)	12.985(3)	2058.8(20)	0.00470	129.7	16.51
6.27	12.562(6)	12.541(4)	12.959(4)	2041.5(9)	[d]	[d]	[d]
3.51 (on release)	12.782(4)	12.755(14)	13.056(3)	2128.7(20)			
0 (released)	13.079(1)	13.050(2)	13.204(1)	2253.6(3)			

[a] The uncertainties in pressure measurement include the precision of the ruby scale and pressure variations during diffraction measurement and are less than ±0.1 GPa

[b] $R = \sum_{i=1}^{n} \{w_i^2 [D_i(\text{predicted}) - D_i(\text{model})]^2\} / \sum_{i=1}^{n} w_i^2 D_i(\text{predicted})^2$

[c] Derived from DLS-modeling (see text)

[d] Did not converge

behavior as observed in thomsonite. Pressure-induced hydration (PIH) and subsequent volume expansion have now been reported in several zeolites including natrolite, mesolite, synthetic potassium-gallosilicate (Lee et al. 2002a,b), and Zn-exchanged LTA (J.A. Hriljac, personal communication). In addition, Belitsky et al. (1992) proposed that edingtonite undergoes one or more reversible phase transition under high water pressures, but there is no experimental evidence or details of the changes. In the case of natrolite, a new fully occupied water site appears upon volume expansion of ca. 2.5% near 1.5 GPa, doubling the crystal water content and expanding the channel along the *a*, *b*-axis. Although built from the same T_5O_{10} tetrahedra unit but with different connectivities between them, the pores in edingtonite and thomsonite already contain more water molecules at ambient conditions than natrolite. When the water contents of these fibrous zeolites (all with framework density around 16 T atoms 1000 $Å^{-3}$) are normalized to 80 framework oxygen atoms; edingtonite and thomsonite have 24 to 32 water molecules, whereas natrolite contains only 16 water molecules below 0.8 GPa and subsequently doubles its water content to 32 near 1.5 GPa. Based on this, PIH is not likely to occur in edingtonite or thomsonite. In addition, the Ba cation located on the twofold axis in edingtonite already adopts a full ten fold coordination with six framework oxygen atoms and four surrounding water molecules under ambient conditions (Galli 1976), analogous to the Na coordination in the PIH state of natrolite. This removes the driving force of increasing the cation coordination through PIH.

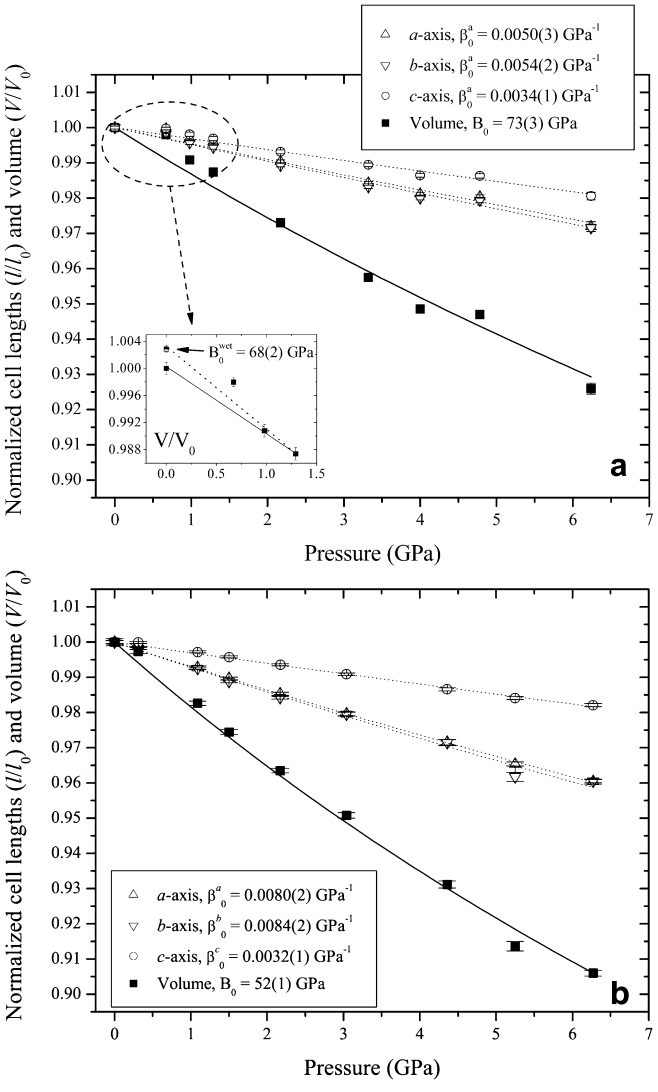

Fig. 3a, b Pressure dependence of the unit-cell edge lengths and volume of **a** edingtonite and **b** thomsonite, normalized to their ambient pressure values. *Continuous lines* are fits to the volume data using second-order Birch–Murnaghan equation of state, and *dotted lines* are guides to the eye (linear compressibilities were obtained from fits to the cell-length data using linearized second-order Birch–Murnaghan equation of state, see text). *Inset in edingtonite* shows details of the normalized volume below 1.5 GPa and the bulk modulus fit using the volume of the wet capillary sample as V_0 (*half-filled square*, see text)

It is known that the number of water molecules absorbed inside zeolitic pores depends on humidity as well as temperature, especially in laumontite and many large pore zeolites such as rho, and X. An increase in the unit-cell volume can be caused by changes in the hydration level under ambient conditions. We have confirmed that the edingtonite sample soaked with the same alcohol and water mixture inside a capillary has a slightly larger unit-cell volume (0.3%) than that of the dry powder (Fig. 3a); the bulk modulus calculated taking the volume of the wet capillary sample as V_0 is 68(2) GPa (within 2σ of the value using V_0 of the dry powder). Some deficiency in the initial hydration level, and subsequent hydration-induced swelling upon soaking the dry sample into the water-bearing pressure medium, is therefore the explanation of the anomaly observed in the pressure–volume data of edingtonite below 1.5 GPa. This may be the phase transition referred to, without further detail, in an earlier work (Belitsky et al. 1992). It is also interesting to note that the edingtonite sample after pressure release shows unit-cell lengths similar to those of the wet powder sample, whereas in thomsonite the values after pressure release are similar to those of the initial dry powder sample before pressure cycle (Table 1). This effect is not seen when a nonpenetrating pressure medium is used, as in the studies of other fibrous zeolites such as scolecite (Ballone et al. 2002; Comodi et al. 2002).

If we compare the normalized unit cell data of edingtonite and thomsonite to those of natrolite above 1.5 GPa (PIH-natrolite), their linear compressibilities along and across the T_5O_{10} tetrahedral chains would represent to some extent the intrinsic pressure responses of each framework resulting from the different connectivities between the chains. Linear compressibility, $\beta_0 = -(\partial l/\partial P)/l_0$, where l_0 is the length of a unit-cell axis at 1 bar (1.5 GPa for natrolite), was calculated by fitting the cell lengths to a linearized second-order Birch–Murnaghan equation of state (Angel 2000). It was found that the compression along the T_5O_{10} tetrahedral chain (*c*-axis) is very similar

(edingtonite, $\beta_0^c = 0.0034(1)$ GPa^{-1}; thomsonite, $\beta_0^c = 0.0032(1)$ GPa^{-1}; PIH-natrolite, $\beta_0^c = 0.0028(1)$ GPa^{-1}) and is the least compressible component in all three frameworks. Thomsonite and PIH-natrolite, however, show a greater compression behavior across the chains (*a*-, *b*-axis) compared to edingtonite; thomsonite, $\beta_0^a = 0.0080(2)$ Gpa^{-1}, $\beta_0^b = 0.0084(2)$ GPa^{-1}; PIH-natrolite, $\beta_0^a = 0.0086(3)$ GPa^{-1}, $\beta_0^b = 0.0091(1)$ GPa^{-1}; edingtonite, $\beta_0^a = 0.0050(3)$ GPa^{-1}, $\beta_0^b = 0.0054(2)$ GPa^{-1}. As a result, the bulk moduli of PIH-natrolite and thomsonite are found to be nearly identical while that of edingtonite is about 40% larger ($K_0^{EDI} = 73(3)$ GPa, $K_0^{THO} = 52(1)$ GPa, $K_0^{PIH-NAT} = 49(1)$ GPa).

As far as the framework is concerned, the smaller linear compression of edingtonite perpendicular to the chain axis may be related to the *0000*-type connectivity of the fibrous chains. In edingtonite, the dense 4-ring tetrahedra of the neighboring fibrous chains are at the same heights in the *ab* plane and, when compressed, will be pushed directly against each other, whereas in thomsonite and natrolite these dense units are staggered along [001] due to the *0022*- and *2460*-type connectivity, respectively. Therefore the compression results in bending the relatively weak T–O–T angle connector between the neighboring chains (Fig. 2). The in situ high-pressure data from edingtonite and thomsonite, however, were not of sufficient quality to allow detailed structural analysis using Rietveld methods. This was due, in large part, to the severe texture observed in several loadings that led to poor powder averaging. Instead, we have used a distance least-squares (DLS) framework minimization technique in order to model the high-pressure framework using the observed pressure-cell length data. A weighting scheme of $W(T–O):W(O–O):W(T–T) = 10:2:1$ was used along with ideal interatomic distances of Si–O = 1.62 Å, Al–O = 1.75 Å, O–O = 2.66 Å (on Si tetrahedra) and 2.86 Å (on Al tetrahedra) and O–T–O and T–O–T angles for framework aluminosilicate systems (109.5° and 145°, respectively). This assumes relatively rigid tetrahedra and is therefore sensitive to the T–O–T angle variations. The normalized values of the chain-bridging T–O–T angles, derived from the DLS-minimized frameworks, are reported in Table 1 and plotted in Fig. 4. The changes of these angles generally agree with the experimentally observed linear compression behaviors and show greater rigidity for the edingtonite framework than thomsonite. In addition, the resulting overall chain rotation angle, ψ, when represented by the mean of the angles between the sides of the quadrilateral around the T_5O_{10} tetrahedral building unit and the axes of the elliptical channels projected on the (001) plane (Baur et al. 1990), also shows a greater degree of channel distortion and collapse in thomsonite than in edingtonite (Fig. 4). In reality, however, the interplay between nonframework cations, water molecules, and the framework, none of which is part of the DLS minimization, will also be important factors in determining the pressure-driven structural changes, and need to be investigated further.

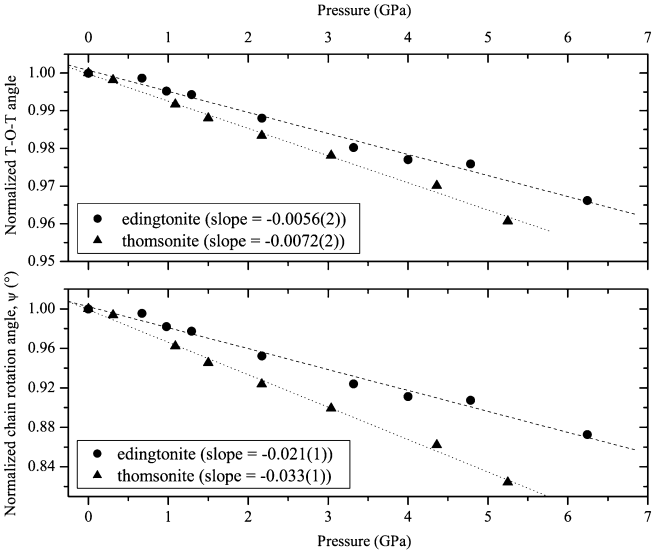

Fig. 4 Pressure dependence of the normalized chain-bridging T–O–T angles and overall chain rotation angles (ψ) of edingtonite and thomsonite, derived from DLS-framework modeling. The actual values are reported in Table 1 and are different from each other due to the different framework topology. *Dotted lines* are linear fits

Acknowledgements This work was supported by an LDRD (Laboratory Directed Research and Development) from BNL (Pressure in Nanopores). J. Hriljac thanks the Royal Society. The authors thank Jeffrey Post of the National Museum of Natural History at the Smithsonian Institution for providing the mineral specimens, Jingzhu Hu of the Geophysical Laboratory of the Carnegie Institute for access to their ruby laser system at beamline X17C and Patrick Woodward of Ohio State University for collecting ambient pressure X-ray powder diffraction data. Research carried out in part at the NSLS at BNL is supported by the US DoE (DE-Ac02–98CH10886 for beamline X7A).

References

Angel RJ (2000) Equations of state. In: Hazen RM, Downs RT, (eds). Reviews in mineralogy and geochemistry: high-temperature and high-pressure crystal chemistry, vol. 41. The Mineralogical Society of America, Washington, DC, p. 35–58

Ballone P, Quartieri S, Sani A, Vezzalini G (2002) High-pressure deformation mechanism in scolecite: a combined computational-experimental study. Am Mineral 87: 1194–1206

Baur WH (1977) Computer simulation of crystal-structures. Phys. Chem. Miner. 2: 3

Baur WH, Joswig W (1996) The phases of natrolite occuring during dehydration and rehydration studied by single crystal X-ray diffraction methods between room temperature and 923 K. N. Jb Miner Mh 4: 171–187

Baur WH, Kassner D, Kim C-H, Sieber NH (1990) Flexibility and distortion of the framework of natrolite: crystal structures of ion-exchanged natrolites. Eur J Mineral 2: 761–769

Bazhan IS, Kholdeev OV, Fursenko BA (1999) Phase transformations in scolecite at high hydrostatic pressures. Doklady Akad Nauk 364: 97–100

Belitsky IA, Fursenko BA, Gubada SP, Kholdeev OV, Seryotkin YV (1992) Structural transformations in natrolite and edingtonite. Phys Chem Minerals 18: 497–505

Bell PM, Mao HK (1979) Absolute pressure measurements and their comparison with the ruby fluorescence (R1) pressure scale to 1.5 Mbar. Carnegie Inst Washington Year Book, 78, p. 665–669

Breck DW (1984) Zeolite molecular sieves. Krieger, Malabar, Florida

Comodi P, Gatta GD, Zanazzi PF (2002) High-pressure structural behavior of scolecite. Eur J Mineral 14: 567–574

Galli E (1976) Crystal structure refinement of edingtonite. Acta Crystallogr (B)32: 1623

Gillet P, Malezieux J-M, Itie J-P (1996) Phase changes and amorphization of zeolites at high pressures: the case of scolecite and mesolite. Am Mineral 81: 651–657

Goryainov SV, Smirnov MB (2001) Raman spectra and lattice-dynamical calculations of natrolite. Eur J Mineral 13: 507–519

Gramlich V, Meier WE (1971) The crystal structure of hydrated NaA: A detailed refinement of a pseudosymmetric zeolite. Z Kristallogr 133: 134–149

Hazen RM (1983) Zeolite molecular-sieve 4 A – anomalous compressibility and volume discontinuities at high pressure. Science 219: 1065–1067

Hazen RM, Finger LW (1982) Comparative crystal chemistry. Wiley, New York

LeBail A, Duroy H, Fourquet JL (1988) Ab-initio structure determination of $LiSbWO_6$ by powder X-ray diffraction. Mat Res Bull 23: 447–452

Lee Y, Hriljac JA, Vogt T, Parise JB, Artioli G (2001a) First structural investigation of a super-hydrated zeolite. J Am Chem Soc 123: 12732–12733

Lee Y, Reisner BA, Hanson JC, Jones GA, Parise JB, Corbin DR, Toby BH, Freitag A, Larese JZ, Kahlenberg V (2001b) New insight into cation relocations within the pores of zeolite rho: in situ synchrotron X-ray and neutron powder diffraction studies of Pb- and Cd-exchanged rho. J Phys Chem (B)105(30): 7188–7199

Lee Y, Vogt T, Hriljac JA, Parise JB, Artioli G (2002a) Pressure-induced volume expansion of zeolites in the natrolite family. J Am Chem Soc 124: 5466–5475

Lee Y, Vogt T, Hriljac JA, Parise JB, Hanson JC, Kim SJ (2002b) Non-framework cation migration and irreversible pressure-induced hydration in a zeolite. Nature 420: 485–489

Lemonnier M, Fourme R, Rosseaux F, Kahn R (1978) X-ray curved-crystal monochromator system at the storage ring DCI. Nucl Instrum Methods 152: 173–177

Meier WH, Villiger H (1969) Abstandsverfeinerung zur Bestimmung der Atomkoordinaten idealisierter Geruestrukturen. Z Kristallogr 129: 411–423

Merrill L, Bassett WA (1974) Miniature diamond anvil pressure cell for single-crystal X-ray diffraction studies. Rev Sci Instrum 45: 290–294

Moroz NK, Kholopov EV, Belitsky IA, Fursenko BA (2001) Pressure-enhanced molecular self-diffusion in microporous solids. Microporous Mesoporous Mater 42: 113–119

Norby P, Poshni FI, Gualtieri AF, Hanson JC, Crey CP (1998) Cation migration in zeolite: an in-situ powder diffraction and MAS NMR study of the structure of zeolite Ca(Na)-Y during dehydration. J Phys Chem (B)102: 839

Olson DH, Kokotailo GT, Lawton SL, Meier WM (1981) Crystal-structure and structure-related properties of ZSM-5. J Phys Chem 85: 2238–2243

Parise JB, Gier TE, Corbin DR, Cox DE (1984) Structural changes occurring upon dehydration of zeolite-rho – a study using neutron powder diffraction and distance-least-squares structural modeling. J Phys Chem 88: 1635–1640

Smith GC (1991) X-ray imaging with gas proportional detectors. Synch Rad News 4: 24–30

Smith JV (1983) Enumeration of 4-connected 3-dimensional nets and classification of framework silicates: combination of 4–1 chain and 2D nets. Z Kristallogr 165: 191–198

Taylor WH, Meek CA, Jackson WW (1933) The structures of the fibrous zeolites. Z Kristallogr 84: 373